Nonlinear hybrid plasmonic slot waveguide for second-harmonic generation

Haozhi Yin (尹昊智), Yumin Liu (刘玉敏)*, Zhongyuan Yu (俞重远), Qiang Shi (石　强),
Hui Gong (宫　慧), Xiu Wu (吴　秀), and Xin Song (宋　鑫)

State Key Laboratory of Information Photonics and Optical Communications,

Beijing University of Posts and Telecommunications, Beijing 100876, China

*Corresponding author: microliuyumin@hotmail.com

A nonlinear hybrid plasmonic slot waveguide composed of periodically poled lithium niobate (PPLN) and two separated silver films is investigated. The effective refractive index, propagation length, and energy confinement of the hybrid anti-symmetric mode in this waveguide are calculated using the structure parameters at the fundamental wavelength of $\lambda = 1550$ nm and its second harmonic (SH) $\lambda = 775$ nm. Through the above indices, coupling efficiency (maximum SH conversion efficiency during propagation) and peak position (propagation location of the conversion efficiency) of SH generation are analyzed. Finally, higher conversion efficiency can be achieved at a shorter propagation distance by changing the waveguide into a tapered structure.

OCIS codes: 190.2620, 240.6680, 230.7370.

doi: 10.3788/COL201311.101901.

Second-harmonic generation (SHG)[1] is a fundamental nonlinear optical process that can simultaneously consume fundamental frequency (FF) and second harmonic (SH). Achieving SHG requires that light is held and that the dimension of the system have efficient intensity. As the sub-wavelength light confinement and local field enhancement of surface plasmon polaritons (SPPs)[2], numerous proposed waveguide structures based on SPP have been employed in recent years to investigate SHG, such as nonlinear slot waveguide[3,4], nonlinear long-range SPP waveguide (LRSPP)[5], and hybrid SPP waveguide[6−8]. Ruan *et al.*[9] investigated a metallic slot waveguide to enhance the efficiency of THz conversion and provide extensive theoretical analysis. In addition, SH conversion based on SPPs through quasi-phase matching (QPM) was studied[10]. Lu *et al.*[7] utilized a hybrid nonlinear plasmonic waveguide to attain an efficient SHG in which the air gap has twofold roles in confining the optical-field and reducing mode loss.

Three fundamental factors directly affect the conversion process of SHG in the abovementioned systems, namely, propagation loss, couple coefficient, and phase matching. For phase matching, several approaches have been suggested and demonstrated, including birefringence[11], quadratic phase matching[12], and QPM. Birefringence does not generally include collinear phase matching, whereas quadratic phase matching requires a strict waveguide size under a fixed wavelength. Given the maturity of the QPM technology in nano-optics, ideal phase matchinG can be achieved through the periodically poled LiNbO₃ (PPLN)[10] with a large nonlinear coefficient d_{33}. In the plasmonic system, the confinement of the metallic structure results in a satisfactory modal profile overlap; however, this same case inevitably introduces a higher loss compared with fundamental frequency and second harmonic. Thus, a trade off should be considered.

In this letter, a nonlinear hybrid plasmonic slot waveguide that introduces a dielectric gap in the metal–insulator–metal (MIM) plasmonic slot waveguide is demonstrated, with the PPLN as the waveguide material. Firstly, the geometry and mode of the structure are presented. Subsequently, the influences of the waveguide parameters on the effective refractive index, propagation length, and energy confinement are discussed. Following the above discussion, SHG is analyzed, including coupling efficiency (maximum SH conversion efficiency during propagation) and peak position (location where SH achieves the maximum) by numerically solving for the coupling wave equations. These two indices directly reflect the conversion efficiency and conversion rate. Furthermore, the waveguide is consequently changed into a tapered structure[13] to improve the second-harmonic conversion process. All simulation processes employ the numerical FEM method at communication wavelength of 1550 nm and SH at 775 nm.

As shown in Fig. 1, the structure of the waveguide is a PPLN that has a square cross-section located between two equal altitude silver films. These three parts are placed into a vacuum and Separated with two gaps. The square angles of the LiNbO₃ (LN) and the relevant corner of the silver films are smoothed to obtain fillets, with $r = d/5$ (d is the length of the side of the LN part), considering the simultaneous reduction of the loss to a certain degree and maintaining field confinement. The
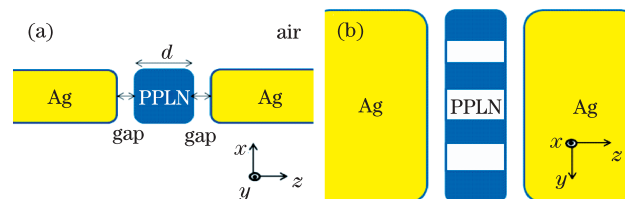

Fig. 1. (Color online) Structure of the nonlinear hybrid plasmonic slot waveguide. (a) Cross-section; (b) vertical view.

relevant opticals are $\varepsilon_m = -126 + i3.4$, $[\varepsilon_x, \varepsilon_y, \varepsilon_z] = [4.89, 4.89, 4.57]$ for FF and $\varepsilon_m = -30.77 + i0.42$, $[\varepsilon_x, \varepsilon_y, \varepsilon_z] = [5.1, 5.1, 4.74]$ for SH. The c-axis of LN is oriented along the z-axis, with its periodically poled domain wall placed along the y-axis. Silver is chosen as the metal film because it has lower light attenuation at the communication wavelength of 1 550 nm and SH of 775 nm.

Two main guide modes are employed for MIM and metal-multi-insulator-metal (MMIM) plasmonic slot waveguides, namely, anti-symmetric SPP (a_{spp}) mode and symmetric (s_{spp}) mode[14,15]. In the proposed structure, these two modes also exist. Given that the electric field component in the direction of propagation E_y is directly relevant in driving plasma oscillations, E_y and hybrid theory[16] are referred to, which are defined as anti-symmetric hybrid mode (shown in Fig. 2(c)) and symmetric hybrid mode, respectively. Considering that the anti-symmetric hybrid mode is the fundamental mode and possesses better properties[15], this mode is only investigated in the latter part of the letter, without special emphasis.

The lateral electric field E_z distribution of FF and SH are shown in Figs. 2(a) and (b), respectively, with the following sample structure parameters: $d = 500$ nm and gap = 50 nm. Field distribution in the air gap is strong for FF, and more fields are concentrated inside the LN portion for the SH, which indicates a strong surface plasma excitation at the two air-metal interfaces of FF and a relatively weaker interaction of SH. This state results in the SPP-like hybrid mode of FF and the waveguide-like hybrid mode of SH. The normalized modal profile of the lateral electric field component E_z of the two wavelengths (shown in Fig. 2(d)) indicates the modal overlap of FF and SH, which is directly related to the coupling coefficient.

In this structure, the mode is formed by the interaction of single SPPs that are associated with the excitation of the two metal-insulator interfaces. The effective refractive index of each interface can be written as

$$n_{\mathrm{spp}} = \left[(\varepsilon_d \cdot \varepsilon_m) / (\varepsilon_d + \varepsilon_m) \right]^{1/2}. \qquad (1)$$

Due to the existence of the air gaps, the interface is composed of metal and air; as such, can be given by $n_{\mathrm{FFL}} = 1.004 + i1.051 \times 10^4$ for the FF wave and $n_{\mathrm{SHL}} = 1.017 + i2.330 \times 10^4$ for the SH wave. When the air gaps between the waveguide and the metal are absent, the effective refractive index will be $n_{\mathrm{FFH}} = 2.256 + i0.0012$ for the FF wave and $n_{\mathrm{SHH}} = 2.472 + i0.0033$ for the SH wave considering the direct interaction between the metal and the LN parts. Owing to the influence of the fillets, the structure is not transformed into a true slot waveguide, so that the limitation of the real part of n_{effH} and n_{effL} are somewhat different from n_{H} and n_{L}, which have been previously calculated.

Figure 3 shows the real part of the effective refractive index of (a) FF and (b) SH and the respective propagation lengths of (c) FF and (d) SH. The black line in each subgraph represents a corresponding MIM plasmonic waveguide. These lines indicate that the introduction of the low refractive index gap modifies the basic properties of the waveguide compared with the MIM

structure; not only is the real part of the effective refractive index pulled down, but the propagation length is also largely enhanced. This phenomenon is due to the gaps that separate LN from the metal, preventing direct interaction between the two parts. All effective refractive indexes gradually converge to limit the value, with the gap gradually changing from zero or infinity.

The variation in energy proportion in each part is crucial in the evaluation of the properties of the waveguide. Figure 4 shows the energy variation for (a) FF and (b) SH in terms of the structure parameters.

The electromagnetic energy density $W(\sigma)$(per unit length along the direction of propagation) is given by

$$W(\sigma) = \frac{1}{2} \left(\frac{\mathrm{d}(\varepsilon(\sigma)\omega)}{\mathrm{d}\omega} |E(\sigma)|^2 + \mu_0 |H(\sigma)|^2 \right). \qquad (2)$$

Due to the relatively weaker plasmonic effect, the energy in the metal is always at a low level, and the energy confinement behavior of the LN and the gap demonstrate
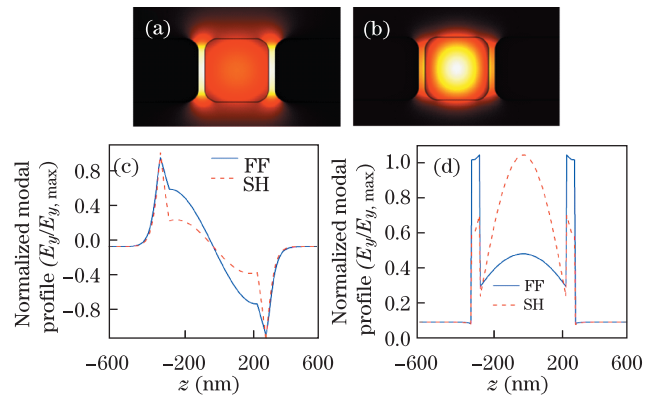

Fig. 2. (Color online) Lateral electric field component E_z distribution of (a) FF and (b) SH; normalized modal profile of (c) longitudinal electric field component E_y and (d) lateral electric field component E_z. Sample structure size. $d = 500$ nm, gap = 50 nm.
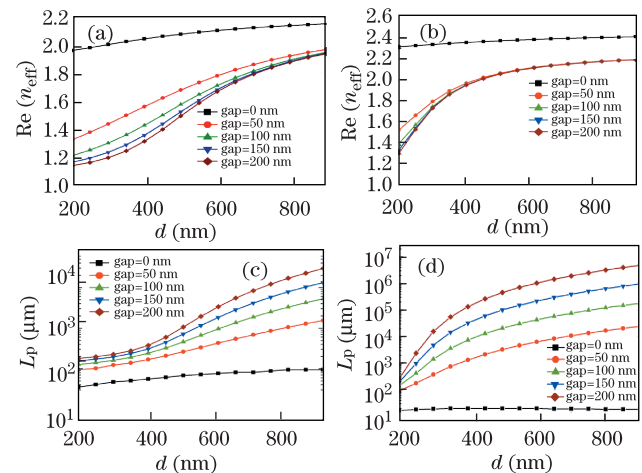

Fig. 3. (Color online) Real part of the effective refractive index of (a) FF and (b) SH. Propagated length of (c) FF and (d) SH. The black line represents the relevant MIM waveguide.
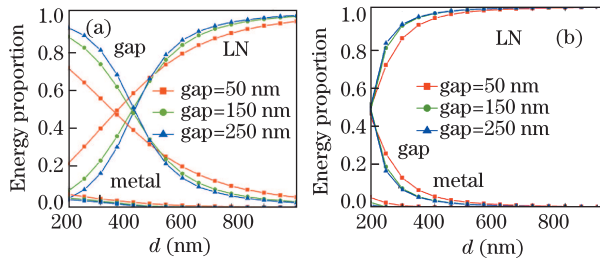
Fig. 4. (Color online) The proportion of energy in each part of (a) FF and (b) SH with the gap fixed at 50 (red), 150 (green), and 250 nm (blue).

invariably opposite trends. For the fixed gap, the energy proportion in the LN part increases along with the growth in the size of LN, whereas the energy proportion of the gap goes to the cross-current. When the size of the LN part is small (that is, less than 450 (FF) and 200 nm (SH)), the energy proportion of the gap becomes dominant. With the increase of the size of the gap, this attribute is further enhanced, whereas the energy in LN is reduced under the same circumstances. When the size of LN is relatively large (that is, greater than 450 (FF) and 200 nm (SH)), the trend of energy variation is reversed in two parts, with the growth of the gap opposite the small size. When LN is small, it carries minor energy, and the guide mode is SPP-like. Furthermore, major energy is concentrated in the gap, so the larger gap can capture more energy. However, when the LN is large, the high refractive index results in a strong restrictive capacity of energy, and the energy proportion of LN becomes dominant. Thus, the larger the gap, the more energy gaps it confines.

During phase matching, coupling efficiency directly results in mode loss and modal overlap. With a small LN (200 nm < d < 450 nm), the variation in energy proportion of the two wavelengths leads to the modal overlap becoming smaller with the growth of the gap. As the loss is always relatively large within this range, the resulting coupling efficiency cannot meet the goal of the study (that is, coupling efficiency can be enhanced along with the growth of the gap). The LN part has to be larger than 450 nm to obtain a high coupling efficiency. When d < 200 nm, the modes of the two wavelengths are both SPP-like, so the coupling coefficient may be sufficiently large, such as dielectric-loaded surface plasman–polariton waveguides (DLSPPW)[17]. However, the coupling coefficient may not compensate for the large loss; thus, this coefficient is excluded from our consideration.

Mode area reveals the energy confinement capacity of this hybrid plasmonic waveguide. The normalized modal area of FF is shown in Fig. 5. The red line reflects that d = 400 nm cannot confine the energy well with the increase in the size of the gap. For the larger sizes of LN, the normalized modal area reaches each unchanged value. This phenomenon can be explained by the behavior of energy confinement discussed above, as the energy in the gap grows with the increase in the gap. When d = 400 nm, the structure cannot confine energy well, leading to more field concentration in the gap and even leakage to the background (inset (a)) compared with the field distribution of d = 500 nm (inset (b)). The normalized

modal area is defined as A_{eff}/A_0, where $A_0 = \lambda_0^2/4$, and A_{eff} is given by[16]

$$A_{\mathrm{eff}} = \int_{-\infty}^{+\infty} W(\sigma)\mathrm{d}\sigma/W(\sigma)_{\mathrm{max}}. \tag{3}$$

The surface integral occurs in every domain in the waveguide cross-section.

Figure 6 shows the intensity evolutions of FF (blue) and SH (red) in the propagation process at d = 500 nm and gap = 50 nm. The coupling equations are given by[8]

$$\frac{\partial A_{\mathrm{FF}}}{\partial y} = -\frac{\alpha_{\mathrm{FF}}}{2}A_{\mathrm{FF}} + i\frac{\omega\varepsilon_0}{4}\kappa_{\mathrm{FF}}A_{\mathrm{FF}}^*A_{\mathrm{SH}}e^{i(\beta_{\mathrm{SH}}-2\beta_{\mathrm{FF}})y},$$
$$\frac{\partial A_{\mathrm{SH}}}{\partial y} = -\frac{\alpha_{\mathrm{SH}}}{2}A_{\mathrm{SH}} + i\frac{\omega\varepsilon_0}{4}\kappa_{\mathrm{SH}}A_{\mathrm{FF}}A_{\mathrm{SH}}e^{-i(\beta_{\mathrm{SH}}-2\beta_{\mathrm{FF}})y},$$
$$\tag{4}$$

where β and $\alpha/2$ are related to the real and imaginary parts of the wave vectors, respectively, and $k = \beta + i\alpha/2 = k_0 \cdot n_{\mathrm{neff}}$ and A are the amplitudes of the electric field. The coupling coefficients are defined as $\kappa_{\mathrm{FF}} = \int \chi : \overrightarrow{E}_{\mathrm{FF}}\overrightarrow{E}_{\mathrm{FF}} \cdot \overrightarrow{E}_{SH}^* \cdot d\sigma$ and $\kappa_{\mathrm{SH}} = \int \chi : \overrightarrow{E}_{SH} \overrightarrow{E}_{\mathrm{FF}}^* \cdot \overrightarrow{E}_{\mathrm{FF}}^* \cdot d\sigma$, where $\overrightarrow{E}_{\mathrm{FF}}$ and $\overrightarrow{E}_{\mathrm{SH}}$ are normalized mode profiles that follow the normalized equation $\int \frac{1}{2}\left(\rightarrow E \times \overrightarrow{H}\right) \cdot d\sigma = 1$.
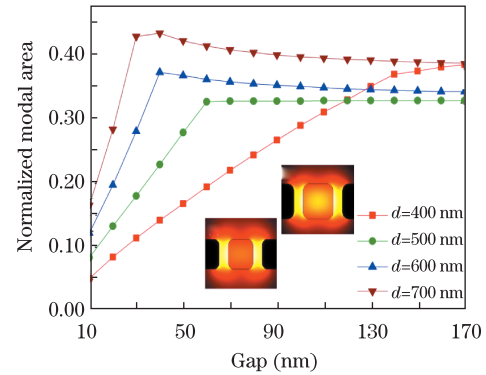

Fig. 5. (Color online) Normalized modal area (NMA) of the FF contrast different sizes of the LN part in terms of gap. The insets show the mode field distribution at gap = 150 nm, with (a) d = 400 nm and (b) d = 500 nm.
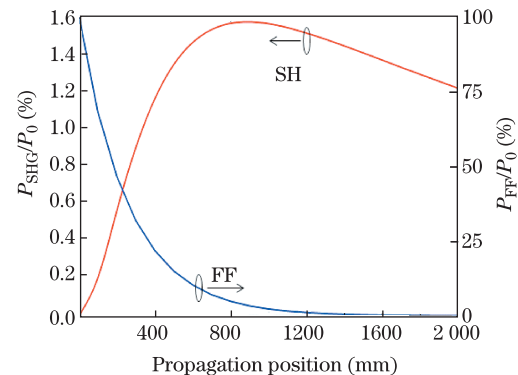

Fig. 6. (Color online) Intensity evolutions of FF (blue) and SH (red) in the propagation process (d=500 nm, gap=50 nm).

All surface integrals occur over the entire waveguide cross-section. The power of incident light is set as 1 W. The mismatch in the wave vector $\Delta\beta = \beta_{SH} - 2\beta_{FF}$ can be compensated by the PPLN whose poling period Λ is calculated by $G = 2\pi/\Lambda = \Delta\beta$, where G is the reciprocal vector of LN. FEM is used to compute for the electric field distribution of FF and SH and their respective n_{eff}. After normalizing the field, the coupling coefficients of FF and SH are computed, and all indices are substituted into Eq. (3), yielding the amplitude of the two signals with the variation of the propagation length.

Figure 7 (a) reveals the coupling efficiency (that is, the maximum SH conversion efficiency during propagation) and (b) the peak position (that is, the emerging propagation position of coupling efficiency) with gaps of 400 (black), 500 (red), and 600 nm (blue). The black line ($d = 400$ nm) confirms the discussion above, that is, although the gap growth results in loss drop off, it cannot compensate the reduction of the coupling coefficient. Therefore, when d is small, increasing the gap does not contribute to the coupling efficiency. For larger sizes ($d = 500, 600$ nm), coupling efficiency increases when the thickness of the gap is increased, and the peak position of the SH increases consistently. Although the coupling efficiency rapidly increases, the peak position emerges at an even further distance at the same time, which may be beyond the practical requirement. For the fixed gap, the larger waveguide size leads to a large coupling efficiency, but requires a longer conversion length.

Furthermore, a tapered structure plasmonic waveguide is proven to possess a self-focusing property, as the enhancement of the local field can compensate for the loss of the system[13]. In this research, a similar structure is designed to maximize the higher coupling efficiency of a larger waveguide and the shorter coupling length of a smaller waveguide to improve performance, as shown in the inset of Fig. 8 (a). The size of LN at the input port is 600 nm and the output port is 400 nm. By modifying the length of the waveguide to acquire a different slope, the gaps remain unchanged in this process. The coupling efficiency and peak position of this waveguide are shown in Figs. 8(a) and (b), respectively, in terms of the gap with different slopes. Although the slope of the small gap is changed, the conversion property obviously remains unimproved (that is, in relation to both coupling efficiency and peak position), given that the gap is not large enough for the difference of the coupling efficiency in the different sizes of LN. Likewise, the coupling efficiency can be replaced by a common waveguide (the
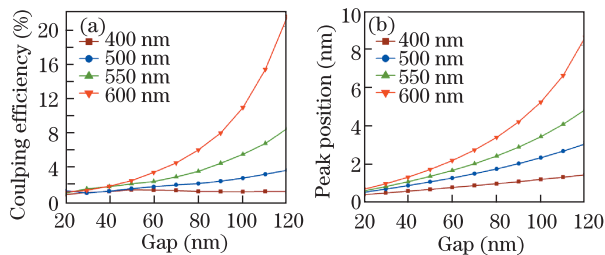

Fig. 7. (Color online) (a) Coupling efficiency (the maximum SH conversion efficiency during propagation) and (b) peak position (the emerging propagation position of the coupling efficiency).
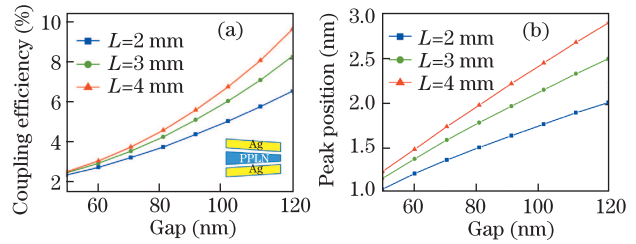

Fig. 8. (Color online) Tapered waveguide (a) coupling efficiency and (b) peak position; L represents the whole waveguide length.
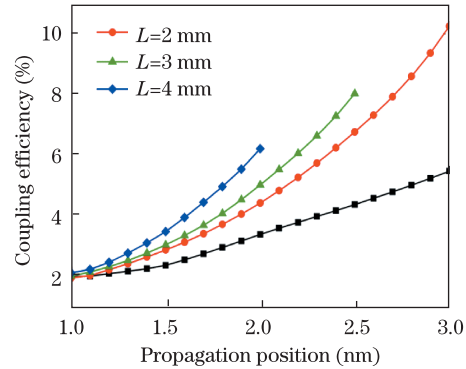

Fig. 9. (Color online) Coupling efficiency in terms of propagation position and maximum common waveguide (black line) compared with the three tapered structures ($L = 2, 3, 4$ mm).

waveguide discussed above) of a particular size, e.g., $L = 3$ mm, gap $= 60$ nm for the tapered waveguide as opposed to the $d = 550$ nm, gap $= 70$ nm for the common waveguide. However, a series that has a higher coupling efficiency can be obtained in a short length in contrast to the common waveguide when the gap is large. For example, within 3 mm from the common waveguide, the coupling efficiency is no more than 6%, whereas the tapered structure can reach 9.5% ($L = 4$ mm, gap $= 120$ nm) at even shorter length. Within 2.5 mm, the tapered structure can reach 8.1% ($L = 3$ mm, gap $= 120$ nm), as opposed to the common waveguide that reaches less than 4.5%. In this manner, the conversion rate is efficiently controlled, so the trade off between coupling efficiency and propagation length can be adjusted depending on the practical application.

To better illustrate the improvement achieved through this method, the coupling efficiency of the different waveguide structures is shown in Fig. 9 as a function of the propagation position. The black line represents the maximum coupling efficiency of the different structure parameters at each propagation position for the common waveguide (400 nm $\leq d \leq$ 600 nm, 40 nm $\leq$ gap $\leq$ 120 nm). The three colored lines represent the tapered waveguide of the different slopes. The truncation of the blue line ($L = 2$ mm) and the green line ($L = 3$ mm) are due to the limitation of the length of the waveguide. The gap range is calculated (gap $\leq$ 120 nm), so a more preferable coupling efficiency can be derived when the gap continually increases within the range of the entire waveguide length.

In conclusion, this research investigates a nonlinear hybrid plasmonic slot waveguide. The properties of the waveguide's anti-symmetric mode, including effective refractive index, propagation length, energy confinement

and SHG, are discussed in terms of waveguide structure parameters. Under this structure, good energy confinement and coupling efficiency can be achieved by introducing and tuning low refractive index gaps. Furthermore, by changing the waveguide into a tapered structure, a series with considerable conversion efficiency within a shorter propagation length can be obtained (that is, 9.5% at 2.9 mm), which cannot be attained by the original waveguide (within 3 mm greater than 6%). The tapered structure combines the higher conversion efficiency of the larger waveguide with the shorter propagation distance of the smaller waveguide. Finally, an intuitive comparison is made among the coupling efficiencies of several waveguide structures at each propagation position. Findings show that the sharper structure results in a higher coupling efficiency that can be achieved at a fixed propagation position. At the same time, this sharper structure is restricted by the entire waveguide length. Therefore, this structure may be useful in some practical applications in optical signal transportation and manipulation.

References

1. R. W. Boyd, *Nonlinear Optics* (Elsevier Science, 2003).
2. A. R. Davoyan, I. V. Shadrivov, and Y. S. Kivshar, Opt. Express **16,** 21209 (2008).
3. A. R. Davoyan, I. V. Shadrivov, and Y. S. Kivshar, Opt. Express **17,** 4833 (2009).
4. M. L. Brongersma and V. M. Shalaev, Science **328,** 440 (2010).
5. A. Degiron and D. R. Smith, Phys. Rev. A **82,** 033812 (2010).
6. D. Dai and S. He, Opt. Express **18,** 17958 (2010).
7. F. F. Lu, T. Li, X. P. Hu, Q. Q. Cheng, S. N. Zhu, and Y. Y. Zhu, Opt. Lett. **36,** 3371 (2011).
8. F. F. Lu, T. Li, J. Xu, Z. D. Xie, L. Li, S. N. Zhu, and Y. Y. Zhu, Opt. Express **19,** 2858 (2011).
9. Z. Ruan, G. Veronis, K. L. Vodopyanov, M. M. Fejer, and S. Fan, Opt. Express **17,** 13502 (2009).
10. Z. J. Wu, X. K. Hu, Z. Y. Yu, W. Hu, F. Xu, and Y. Q. Lu, Phys. Rev. B **82,** 155107 (2010).
11. H. Ishikawa, Appl. Phys. Express **2,** 042202 (2009).
12. A. R. Davoyan, I. V. Shadrivov, and Y. S. Kivshar, Opt. Express **17,** 20063 (2009).
13. A. R. Davoyan, I. V. Ahadrivov, A. A. Zharov, D. K. Gramotnev, and Yu. S. Kivshar, Phys. Rev. Lett. **105,** 116804 (2010).
14. I. D. Rukhlenko, A. Pannipitiya, and M. Premaratne, Opt. Lett. **36,** 3374 (2011).
15. X. T. Kong, W. G. Yan, Z. B. Li, and J. G. Tian, Opt. Express **20,** 12133 (2012).
16. R. F. Oulton, V. J. Sorger, D. A. Genov, D. F. P. Pile, and X. Zhang, Nature Photon. **2,** 496 (2008).
17. T. Holmgaard and S. I. Bozhevolnyi, Phys. Rev. B **75,** 245405 (2007).